

Automated transportable solar panel array

Group: 7

DESCRIPTION OF OPERATION

Deploying the solar panel mechanism requires interaction with the main operating panel, situated on the base plate oriented towards the rear of the truck (*Figure 2*). Note that - to access the panel, opening the tailgate may be required. To extend the solar array, displace the toggle switch (shown in *Figure 1*) towards the “ON” position and hold in place continuously until fully extended. Displacing the switch towards the “OFF” pole will reverse the direction, retracting the panels into their initial folded state. Returning the switch to the neutral position at any point; or forms of obstruction along the deployment path will both interrupt the sequence. A small lamp is used to indicate to the user whether the mechanism is in motion regardless of direction.

THE OPERATING PANEL

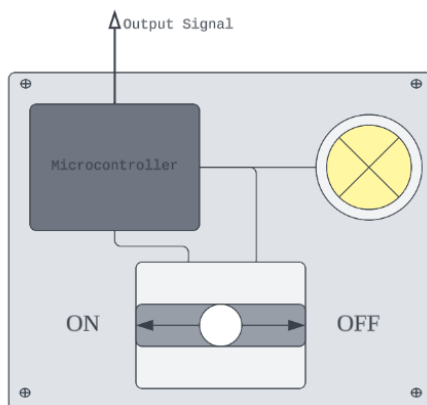


Figure 1: Operating panel interface showing main toggle switch and indicator bulb
Dimensions (6.4 x 3.4cm)

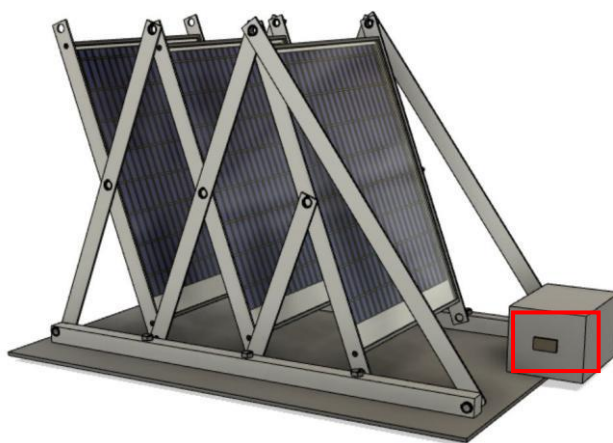


Figure 2: Position on full mechanism affixed to the gearbox, highlighted in red

RATIONALE FOR CHOICE OF SENSORS AND SWITCHES

Initial concepts were to include up to 6 sensors to provide accurate control over the system operation; Including proximity sensors positioned on the leading edge of the panels and several types on the motor shaft to record torque, angular displacement and velocity quantities to compare against normal operating conditions. Identified anomalies to a significant degree i.e.. situations involving wind loading may introduce variation to the angular velocity graph. However, objectives in lowering cost and complexity; in addition to limitations in the length of microcontroller code led to most being omitted from the final design.

The system employs the use of two sensors – one hall sensor and an ultrasonic sensor, both incentivized to meet the requirements while maintaining low cost, and matching low current draw from the main battery of the truck. Each sensor must also physically fit within the space of the baseplate while permitting motion of the panels while in motion;

Hall sensor: Attached to near contact with the gearbox, the hall sensor detects variations in magnetic flux density of a specific gear while in rotation. More specifically, this allows for indirect measurements of angular velocity. If the mechanism encounters a significant shift in angular velocity above a threshold limit (0.3rads^{-1}), the system will terminate regardless of the button state.

Ultrasonic sensor: The ultrasonic sensor is mounted with the emitter upwards at the furthest point along the base plate, and operates by emitting a short pulse of 40kHz waves and detecting obstructions prior to deployment by receiving reflected pulses. This is calibrated for the system by selectively detecting signals within the range of the fully extended array i.e. ($>983\text{mm}$). Likewise, an obstruction will cause the system to terminate.

Figure 3 – Table of convergence for sensor selection

Sensor		Data Utility	Sensitivity/ Resolution	Implement Complexity	Acquired Data Complexity	Cost	Total
Name	Type						
Strain Gauge	Linear distance (Contact)/Strain	4	2	2	4	6	18
Hall Effect	Linear distance / Angular Velocity	9	7	8	6	8	38
Potentiometer	Linear distance / Angular distance	8	8	3	7	5	31
Inductive	Linear Distance	7	8	8	4	4	31
Ultrasonic	Linear distance/Proximity	8	8	8	7	3	34
Optical	Linear distance	6	7	7	7	1	28
DC Generator	Linear Velocity	5	4	1	3	6	18
Gyroscope	Angular Velocity	8	5	8	6	5	32
Accelerometer	Linear Acceleration	4	7	5	8	6	30
Torque sensor	Torque/Linear force/Strain	5	6	4	6	5	26
Thermistor	Temperature	1	7	4	7	7	26
Venturi	Pressure difference	1	2	3	3	4	10

The following sensors were compared by using the selection matrix above (*Figure 3*) considering several selection properties which were regarded as most desirable. As shown, the Hall effect and Ultrasonic sensors scored the highest in context of the system so were incorporated accordingly. A more detailed description of each heading is listed below;

- *Data utility*: Certain types of quantities are not as applicable in the scenario of the deployable array; for instance temperature-related quantities are unlikely to change significantly, and even if so will have intrinsically less influence.
- *Sensitivity/Resolution*: Though different, the two properties can be attributed to a single convergence entry as they are generally correlated. Higher values of either will correspond to better quality of data providing more accurate values that closely represent the environment at a given time.
- *Implementation Complexity*: Smaller, more compact sensors can minimize design tolerances. Additionally, sensors with fewer pins and pre-existing integrated methods of fastening onto the controller are more desirable.
- *Acquired Data Complexity*: Digital data requires less post processing than analogue data, and removes the necessity for a signal conditioner or PWM.
- *Cost*: The average cost of the specific type of sensor - more expensive sensors are less desirable and will increase the cost of the resulting design.
- *Supply(Unlisted)*: Ideally, the same voltage from a single source is sufficient to supply all the sensors to reduce complexity. The demand of sensor input should also remain under the truck's maximum output of 12V.

A justification for each particular switch model and sensor in the mechanism is provided:

Toggle Switch (Stock Number 734-7233):

A single pole double throw manual switch such as the one selected allows the user to manually operate between 2 separate connection and 1 “off” states. This is ideal for the application required as the two active states can be assigned to deploy and retract transitions respectively. Additionally, the component includes a mount to fasten onto the operating panel.

Hall sensor (Stock Number 169-7662):

This specific hall sensor type is compact (4.06 x 3 x 1.57mm), designed to be integrated directly into a PCB. Like most hall sensors, the non-contact mode of measurement is desirable especially in the application of moving components. It provides a digital output, which is easily manipulated without the use of analogue pins in the arduino circuit.

Ultrasonic sensor (Stock Number 215-3181):

Unlike most other ultrasonic based sensors, the 215-3181 is much more affordable costing £2.10, significantly less than externally based sensors and other BBC modules of the same type while compromising resolution and frequency. Adaptation to the microcontroller can be achieved without difficulty as the voltage draw (5V) is within the limit of the truck power supply.

PARTS LIST

RS Catalogue number	Description	Image
734-7233	RS PRO Toggle Switch, Panel Mount, On-Off-On, SPDT, Solder Terminal	
215-3181	Ultrasonic Distance Sensor HC-SR04 5V Version	
169-7662	Honeywell Through Hole Hall Effect Sensor, Digital Output, 3.8 → 30 V dc, 30V	
262-5841	Infineon IMI111T026HXUMA1, BLDC Intelligent Power Module, 600 V 2A 22-Pin, DSO-22	
168-6428	TS272IDT STMicroelectronics, Op Amp, 3.5MHz, 5 → 15 V, 8-Pin SOIC	
761-5463	Texas Instruments LM22675MRE-5.0/NOPB, 1-Channel, Step Down DC-DC Converter 8-Pin, PSOP	
360-7878	RS PRO BA9s Indicator Light, Clear, 130 V, 20 mA, 3000h	

HARDWARE SCHEMATIC DIAGRAM

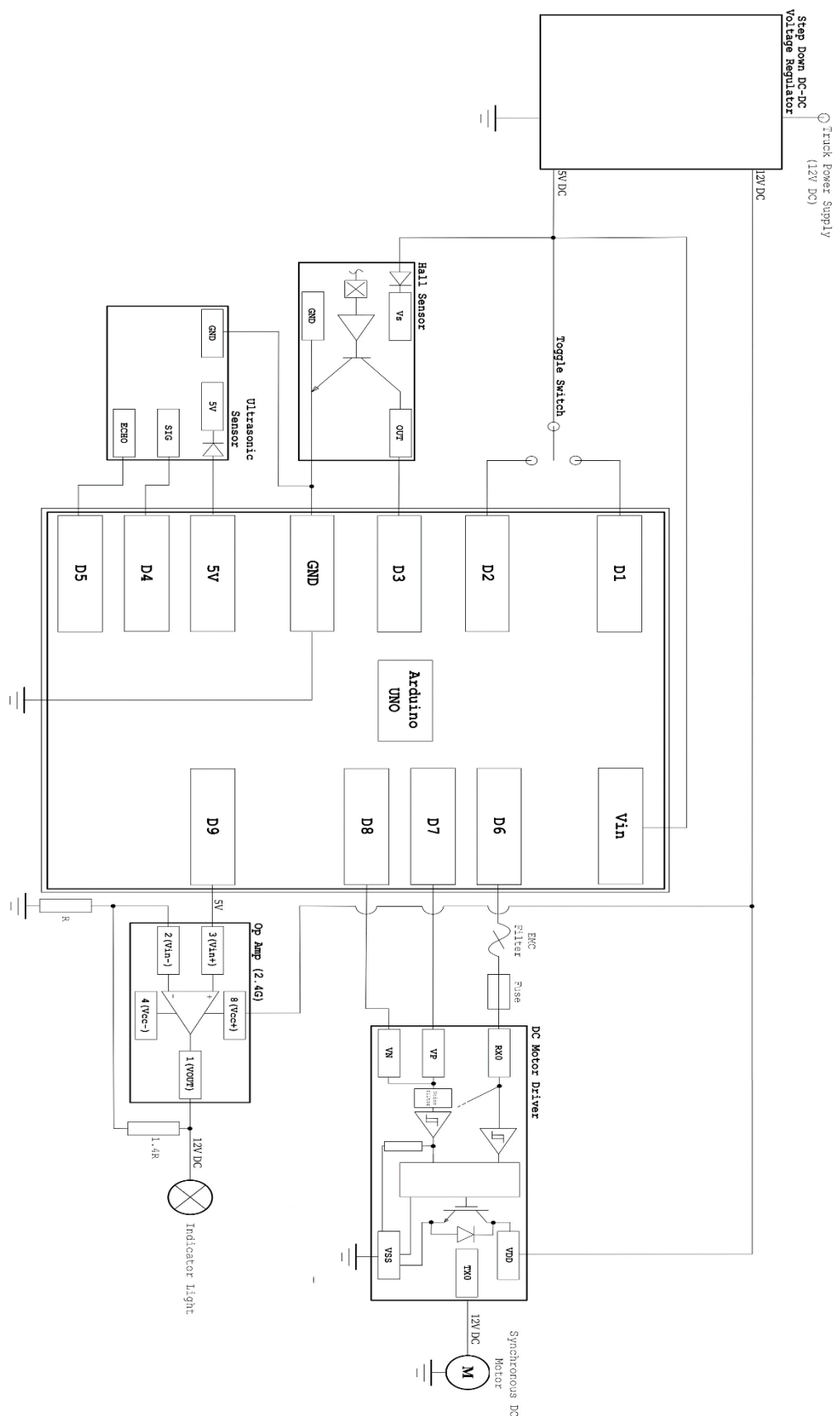


Figure 4 – Hardware Schematic Diagram

STATE TRANSITION DIAGRAM FOR THE SYSTEM

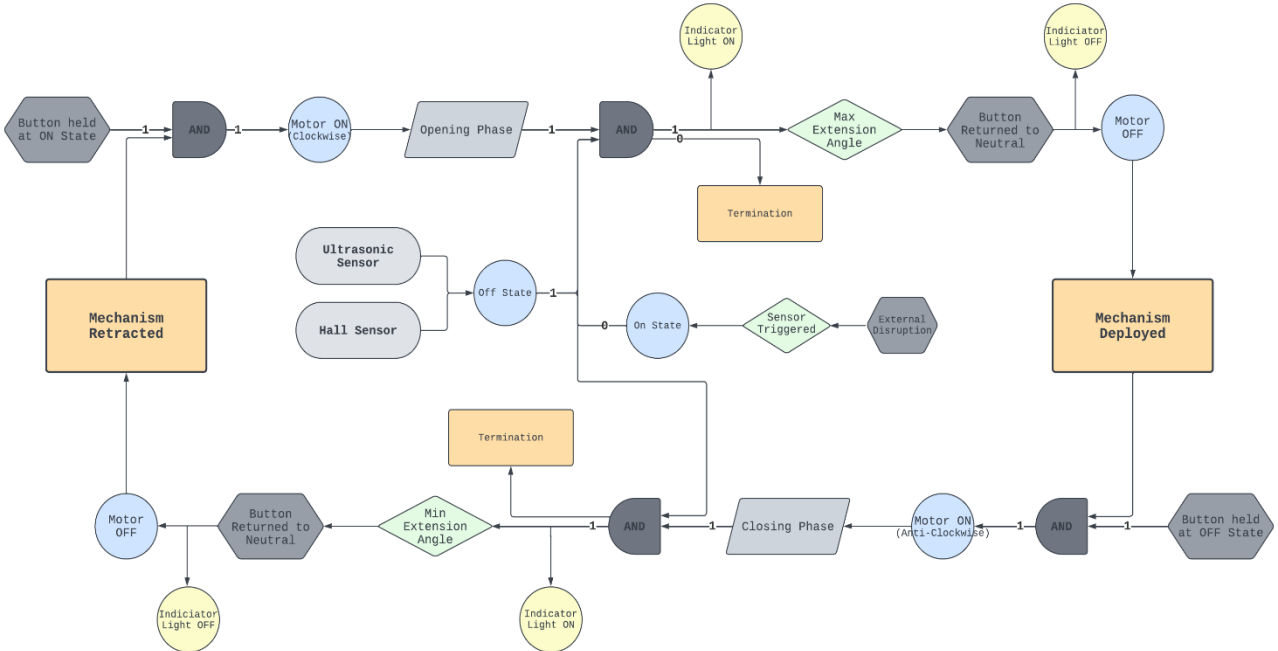


Figure 5 – State Transition Diagram

MICROCONTROLLER SOURCE CODE

```

const int switch_OPEN = 1
const int switch_CLOSE = 2
const int sensor_hall = 3
const int sensor_US_sig = 4
const int sensor_US_echo = 5
const int driver_power = 6
const int driver_direc_CW = 7
const int driver_direc_ACW = 8
const int lamp_PIN = 9
int Open;int Close;int hall_data
float pulse_duration,float US_distance,float lamp_data

void setup(){
  pinMode (switch_OPEN,INPUT);
  pinMode (switch_CLOSE,INPUT);
  pinMode (sensor_hall,INPUT);
  pinMode (sensor_US_sig,OUTPUT);
  pinMode (sensor_US_echo,INPUT);
  pinMode (driver_power,OUTPUT);
  pinMode (driver_direc_CW,OUTPUT);
  pinMode (driver_direc_ACW),OUTPUT;
  pinMode (lamp_PIN,OUTPUT);
}

void loop(){
1 Open = digitalRead (switch_OPEN);
2 Close = digitalRead (switch_CLOSE);
3 hall_data = digitalRead (sensor_hall);
4 lamp_data = analogRead (lamp_PIN);

5 digitalWrite(sensor_US_sig,HIGH);
6 delay(0.01)
7 digitalWrite(sensor_US_sig,LOW);
8 pulse_duration = pulseIn(sensor_US_echo,HIGH);
9 distance = 0.18 * pulse_duration

10 if (Open ==HIGH) {digitalWrite (driver_direc_CW, HIGH); digitalWrite
(driver_direc_ACW,LOW)}

```

```
11 else if ((Close == HIGH) {digitalWrite (driver_dirac_ACW, HIGH); digitalWrite  
(driver_dirac_CW, LOW)}  
12 if ((Open == HIGH)&& (0< distance < 990)) {digitalWrite (driver_power = LOW)}  
13 else if ((Open == HIGH|Close == HIGH) && (hall_data < 0.3)){  
14 digitalWrite (driver_power, HIGH); analogWrite (lamp_PIN,HIGH)}  
15 else if ((Open == LOW) && (Close == LOW)) {  
16 digitalWrite (driver_power = LOW); analogWrite (lamp_PIN,LOW)}  
17 else{}  
18}
```



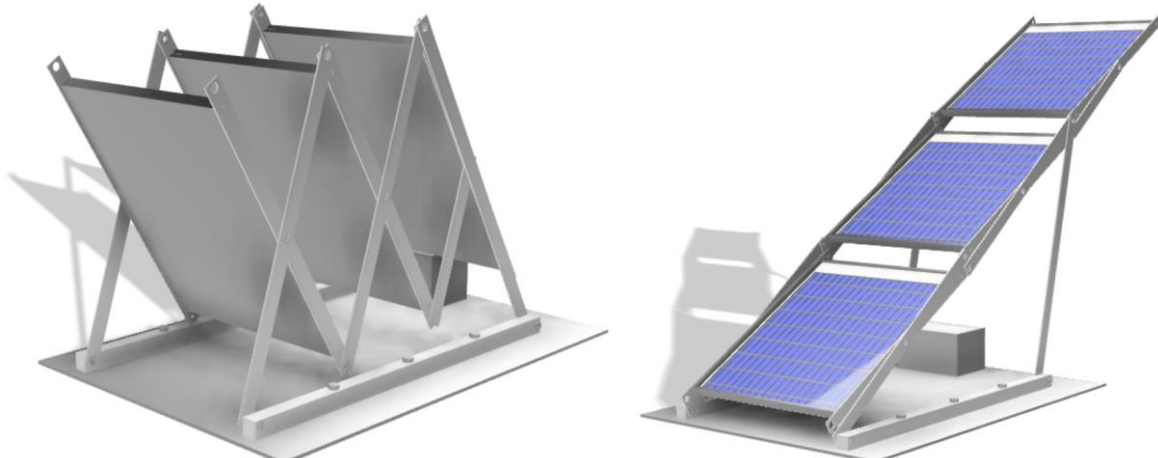
University of
BRISTOL

Mitsubishi L200 Solar Panel Deployment Platform Design Portfolio

Abdullah Monnoo (ul21823), Ibrahim Arekat (wq21745), Kabeer Dayal (pb21912), Ein Lertnawapan (fm21936)

Group 7

Report Date: 04/05/2023



1.0 Project Introduction and Process

This project report covers the detailed design of a flexible solar panel deployment system for a Mitsubishi L200 single-cab pickup truck. The project was initiated in response to the increased demand for solar panel systems because of the Net Zero and Circular Economy initiatives by the government [8]. Acting as the engineering team at Mitsubishi, the aim of the project was to create a proof-of-concept of a solar panel deployment platform within the storage unit of the truck that can be easily transported and enable solar energy generation in remote or isolated locations, thus providing an innovative solution to meet the evolving market demand. The report contains technical information about concept designs, design features, motor and gear selections, and gearbox design. A stakeholder analysis is shown below [10]:

Table 1: Stakeholder Analysis

Key Stakeholder	Description	Priorities
Mitsubishi and Investors	Investors and the company shareholders are important stakeholders as they will be providing the financial resources necessary to develop and produce the solar panel deployment platform. Their interests include profitability, safety, and potential market share. They may also be interested in reputation and therefore the social and environmental impact of the project.	Maximise safety, profitability
Engineering Team	The technical leads of the engineering project should prioritise reliability such that the deployment platform is lightweight, cheap and requires low maintenance.	Reliability, low cost
Customers	Customers will be the ones who use the solar panel deployment platform to generate energy in remote or isolated locations. The customer segment may include individuals and businesses. Their interests include affordability, ease of use, and to generate sufficient energy based on their needs.	Low Cost, easy to use
Government	Regulators are stakeholders who will be responsible for ensuring that the solar panel deployment platform meets relevant government regulations and standards. Their interests include safety, reliability, and compliance with environmental standards. They may also be interested in the potential impact on the local community and environment.	Safety, eco-friendly
Suppliers	Suppliers are stakeholders who will provide the raw materials, components, and equipment necessary to develop and produce the solar panel deployment platform. Their interests include profitability, reliability, and adherence to industry standards.	Profits, industry standard adherence

From this list of stakeholders in table 1, cost, safety, reliability, and ease of use are highly prioritised, especially since Mitsubishi sells within the affordable pickup truck segment. In the report, a few key assumptions were made; The first assumption was that the engineering team tasked to design this mechanism had all components and tools required to make it, readily available. Another assumption was that the same team also has the monetary means to carry out the entire project including research to development and manufacturing.

2.0 PDS

The product design specification (PDS) contains constraints, functional requirements, safety features and other aspects related to the design of the solar panel deployment system, acting as a checklist to ensure that the system meets the intended user needs in an efficient manner. The PDS in table 2 was created from the stakeholder analysis, secondary market research, design brief and engineering intuition.

Table 2: PDS Table

No.	Type	Requirement	Objective	Assessment Method	Priority (1-10)
1	Form	Must be compact enough to fold within truck storage bed	Must have a maximum dimension of 2265mm x 1470mm when undeployed [6]	Run simulation on linkage software	7
2	Form	The mechanism must have smallest undeployed volume while also uncovering most of the solar panel when deployed	Panels should be exposing 90% of its area to the sky and when shut it should have at least half of its open profile.	Run simulation on linkage software	7
3	Form	Solar panels should be within a specified height when undeployed and deployed	The product must have a maximum undeployed height of 1000mm and deployed height of 1600mm	Run simulation on linkage software	6

4	Form	Solar Panels should be a specific angle when deployed	Angle between 25 and 40 degrees to the horizontal to prevent obstruction with roof [6]	Run on simulation	6
5	Functionality	Deployment mechanism must be powered by a standard car battery	It should need a maximum of 12V to be fully deployed [2]	This can be simulated using Arduino	7
6	Functionality	The product should be able to operate consistently in a diverse range of environments and be resistant to wear	Weatherproofing done using gearbox casings. Structure should be able to withstand 120km/h wind without material failure when deployed and must be able to deploy/retract whilst subjected to 32km/h	It must be able to operate at 60°C and withstand torrential rainfall. Winds tested on FEA	6
7	Functionality	The mechanism and its deployment should not be too complex	It must be able to fully deploy using only a singular DC motor and as minimum bars and linkages as possible	Run simulation on linkage software	7
8	Functionality	The mechanism should not need many attachable solar panels to work	It must be able to operate with only a single solar panel, whilst the others can be detachable by customers	Run simulation on linkage software	7
9	Functionality	The system must be compatible with standard solar panel types	The standard solar panels used in this application are 835x670x35mm which the system should be able to fit	The solar panel should be attached during prototyping	8
10	Functionality	The system must be easy to operate and assemble /disassemble for customers with limited technical knowledge	Deployment must be automated with the push of a button	Use automation programming on Arduino to test deployment	8
11	Functionality	Must deploy within a given time limit	15 seconds	Simulate animation on Python	8
12	Functionality	The system should have little to no noise pollution when in deployment motion	Sound should not cross 75-85dB range	Oil-like lubricants should be used to create frictionless-noiseless motion	8
13	Safety	The mechanism should be lightweight- it should not exceed the given mass specifications	It must have a maximum mass of 300kg	Run a fusion model in stress analysis	10
14	Safety	The system must be designed with appropriate safety features to prevent any harm to users or its surroundings	Obstacles should be detected by sensors with distance range of 15mm and a maximum speed of deployment of 0.5m/s	We can test using linkage software	10
15	Safety	Panels should not contact the car roof whilst deployed as it could cause potential damages	Angle and length when deployed should be above the roof with significant margin of error	We can test sensor sensitivity with Arduino	10
16	Safety	It should terminate its deployment if car goes above a specified speed	Above 32km/h deployment should be disengaged. If windspeed is above 32km/h, deployment should be terminated.	We can test sensor sensitivity with Arduino	10
17	Safety	It should terminate its deployment if there is lack of space above	Obstacles such as low-ceiling parking lots and tunnels should be detected to stop deployment	We can test sensor sensitivity with Arduino	10
18	Sustainability	The overall carbon emissions involved must be kept to a minimum	Carbon emissions should be kept at 1.8-2.1 metric tons of CO2 per metric ton of steel produced	Eco-Auditing in material selection	5
19	Sustainability	The system should be designed considering recyclability	Materials should typically have a recyclability of 65%	Material selection	4
20	Maintenance	The system should be easily maintained to reduce downtime	Use minimum hinges and joints, and selection of rust resistant materials	Regularly lubricated, material and other design decisions	7
21	Maintenance	Selected materials of industry standard must be readily available	All materials sourced via reliable manufacturer catalogues	Appropriate market research on material suppliers should be done	6
22	Cost	Overall cost of deployment mechanism should be kept low	Cost cap placed at 700GBP excluding solar panel costs	Effective material, part selection and design decisions	10
23	Longevity	Mechanism should be built to operate for a long lifespan	Should be built to last for 5-7 years: a typical range of time that consumers keep their vehicles	Material selection and design decisions	8

3.0 Concept Design Generation

3.1 Concept 1: Convertible Car Roof Style

The car roof design [12] features three faces on which to mount the solar panels, as shown in figure 1. When undeployed, the faces fold on top of one another, making the profile compact, satisfying requirement 2. This design has the most significant retracted-deployed volume ratio with minimal swept height of 270mm after simulating the mechanism on linkage. It also has no obstruction of the faces, satisfying requirement 2. A significant shortcoming of this concept is that the structure contains additional supporting bars (against requirement 7 and 13). There is a large loading torque on the deploying member, which supports the entire structure. The result would need additional support, folds as well, or rests on the cabin of the truck. The complexity of the design could also impact manufacturing and material costs adversely (against requirement 22).

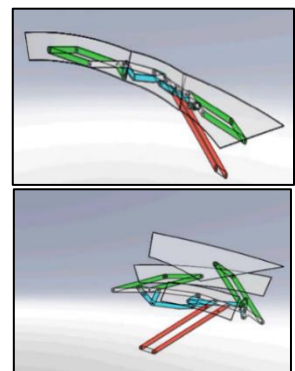


Figure 1: (a) Undeployed and (b) deployed
Convertible Car Roof Design

3.2 Concept 2: Scissor Lift

The scissor lift design [4], shown in figure 2, prioritises simplicity (requirement 20 and 7), in which minimum linkages are used to deploy the solar panels whilst maximising the panel area receiving light. It is compact, easily portable and powered by a single 12 VDC motor (requirement 7), which provides precise movement between the linkages and enables the lift to be operated efficiently. The design has a lifting capacity sufficient for lifting the solar panels to a desired height above the car roof. In a standard scissor lift the lowest points of each member within a cross-cable pair move closer together, decreasing the overall width of the couple whilst increasing its height, to produce a vertical lift. However, in this design, the mechanism is rotated, such that the horizontal length increases, rather than the vertical length. Furthermore, the solar panels are at a tilt angle of 30° to the ground, which is ideal for exposing the surfaces to sunlight (requirement 2).

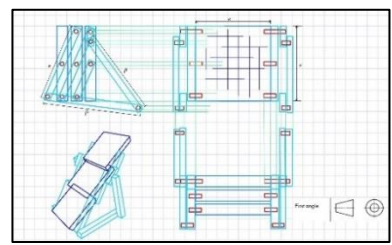


Figure 2: Scissor Lift Technical Drawing

3.3 Concept 3: Cascade Lift

Concept 3 is a Cascade Lift [3], as shown in figure 3, which is a type of lift that extends its members in the vertically. It uses multiple bar-linkages with a pulley system to hoist the given mass upwards. The system would be angled relative to the sun, such that when deployed the solar panels receive maximum sunlight. The features include a gear rack and pinion system attached to a motor to drive the motion of the lift. More members could be added which would further increase the compact form factor when undeployed, (requirement 2) with an incredibly narrow side profile (requirement 1), whilst the front face profile is similarly sized to the other concepts. It has a negligible deployment profile, i.e., it uses all the space that it takes up during deployment. The height of this mechanism is 1500mm (requirement 3). Its complexity stems from having several members and mechanical devices (against requirements 7, 20, 22 and 13).

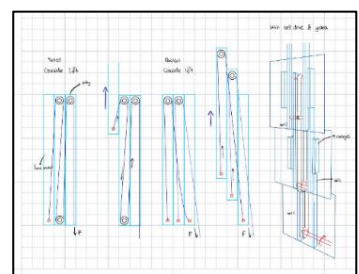


Figure 3: Cascade Lift Technical Drawing

3.4 Concept 4: 6-hinge joint system

The 6-hinge deployment platform in figure 4 is designed to be easy to transport, whilst providing the necessary space and support for solar panels to generate energy. It is designed to fold up into a compact form factor, inspired by a flip phone, such that it occupies minimum retracted volume (requirement 2). The platform enables the panels to pivot about their linkage points and expand to a flat form. The support structure provides a sturdy foundation for the panels, ensuring that they are securely fastened. The flip-hinge is designed to be highly customizable, allowing for up to four panels depending on customer needs, and run on a single 12V DC motor (requirement 5). The platform features an automated tilt mechanism that allows the angle of the solar panels about the pivot to be adjusted for optimal energy production (requirement 4), and a unique form factor that allows it to be stored more efficiently. When folded up, the platform is compact and lightweight (requirements 2 and 13).

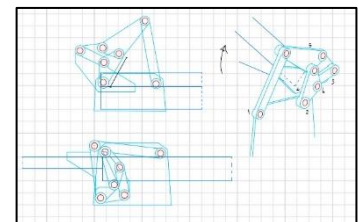


Figure 4: 6-hinge joint

3.5 Concept Selection Criteria

To determine the best design to take forward, a convergence table was created in table 4 to compare each of the four designs based on criterion set out in table 3, based on PDS requirements given in table 2. Each concept was given a final score which was compared with one another to choose the most suitable concept. Within the convergence table, + indicated superior performance than the datum, - indicated inferior performance than datum and S indicated the similar levels of performance as the datum.

Table 3: Selection Criteria Table

Durability: The resistance to wear.	Safety: A smaller deployment profile reduces the risk of failure or complications.	Power generation: The total power output based on the number of solar panels included.
Simplicity: The lower the number of members and joints, the simpler the mechanism.	Stability: The lower the centre of mass of the system, the more stable the deployment.	Cost: The sum of the prices of the constituent components
Ease of manufacture: Dependent on the time, cost and specialisation required to make the individual parts and the final assembly.	Low weight: The total mass in the system based on the number and size of members included.	Volume Ratio: The ratio of volume which encloses the entire system before and after deployment.

Table 4: Controlled Convergence Table

Criteria	Concept 2 (Datum)	Concept 1	Concept 3	Concept 4	Criteria	Concept 2 (Datum)	Concept 1	Concept 3	Concept 4
Low weight	0	+	-	-	Cost	0	+	-	-
Power generation	0	S	S	+	Durability	0	-	-	+
Ease of manufacture	0	S	-	S	Volume Ratio	0	S	-	-
Safety	0	-	-	S	Stability	0	-	-	S
Simplicity	0	-	-	-					
Final score						0	-2	-6	-2
Rank						1	2	3	2

After assessing the concepts, the highest score and rank was achieved by the scissor lift mechanism, with a lower score attributing to a better design. The scissor lift used the least bars and linkages, adhering to low-mass and low-cost priorities compared to the rest. Although the torque requirement was higher compared to the 6-hinge concept, the structure is simpler and cheaper to manufacture whilst being structurally sound.

4.0 Mechanism Design

4.1 Material Selection

According to the PDS, the primary objective was to minimise the mass and cost of the system to achieve points 6 and 16. Thus, the material selection for the beams involved was chosen by applying a multiple conflicting constraint analysis of stiffness and strength. For the beam of length L, experiencing a force F to represent a single member in the system, with stiffness S, the indexes for mass and cost were formed:

$$M_{stiff}^{mass} = \frac{\rho}{\sqrt{E}} \quad [1] \quad M_{strength}^{mass} = \frac{\rho}{\frac{2}{\sigma_y^3}} \quad [2] \quad M_{stiff}^{cost} = \frac{c_m \rho}{\sqrt{E}} \quad [3] \quad M_{strength}^{cost} = \frac{c_m \rho}{\frac{2}{\sigma_y^3}} \quad [4]$$

Using Granta Edupack [1], two graphs were plotted to compare the mass and cost in terms of their stiffness and strength as seen in figures 5 and 6. Using the coupling constant value, a line was drawn across each graph. Here, the box selection method was used with the required stiffness and strength limits. Materials within the box are viable for the beams. To weigh out the importance of each criterion to select the most fitting material, a weighted matrix in table 5 was created which valued each property out of 5 and gave each material a score. The properties were weighted according to the specific PDS requirements, and a final weightage was provided, and calculated through multiplying the rating by the given score. Low Alloy steel clearly had more weightage than the rest, so it was selected as the beam material. Moreover, steel is very sustainable as it can be recycled an infinite number of times without quality deterioration. Because of its inherent strength, less steel needs to be produced and thus results in less CO₂ release (requirement 18 and 19).

Table 5: Weighted Matrix Material Selection

		Cast Iron, Ductile		Low Alloy Steel		Medium Carbon Steel		High Carbon Steel		Cast Al-Alloy		Age Hardened Wrought Al-Alloy		Non-Age Hardened Wrought Al-Alloy	
Criteria	Rating/5	Score/5	Weight	Score/5	Weight	Score/5	Weight	Score/5	Weight	Score/5	Weight	Score/5	Weight	Score/5	Weight
Density (kg/m ³)	3	3	9	2	6	2	6	1	3	4	12	4	12	5	15
Price (GBP/kg)	5	4	20	5	25	5	25	3	15	1	5	1	5	2	10
Yield Strength (MPa)	4	2	8	4	16	4	16	4	16	1	4	5	20	2	8
Tensile Strength (MPa)	2	2	4	4	8	4	8	5	10	1	2	5	10	1	2
Compressive Strength (MPa)	2	4	8	4	8	2	4	5	10	2	4	2	4	1	2
Total			49		63		59		54		27		51		37

4.2 FEA Stress Analysis

To determine the dimensions of the rectangular hind support bars, Fusion 360's FEA stress analysis feature was used to provide a definitive thickness for the rectangular shell design of the bar. Initially, 50mm x 50mm hollow-section bars with a thickness of 6mm were chosen as seen in figure 9 and static stress analysis was carried out on the fully deployed mechanism in Figure 7. According to requirement 13, the bars should be of minimum thickness to reduce mass, whilst providing viable load resistance in harsh conditions. The effects of gravity and windspeed were modelled, with the effect of 120kmph wind to simulate the effects of a hurricane, to provide a worst-case scenario (requirement 6). Safety factor distributions across the bars and Von Mise's stress were found and it was concluded that the two hind support bars which connected the base bars to the panels were over-engineered. Another FEA stress analysis was carried out with less material usage to reduce cost and weight. As geometry iteration, a steel strip of 50mm x 6mm cross-section was used. The lowest safety factor experienced by the strip was 3.058 as in figure 8. The rest of the bars signified safety factors between 5-13 indicating sufficiently safe reinforcement. Thicknesses below 6mm lowered the safety factor down to 0-1, which was highly unsafe.

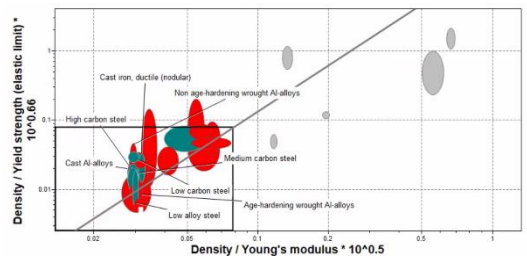


Figure 5: Mass Stiffness-Strength Constraints

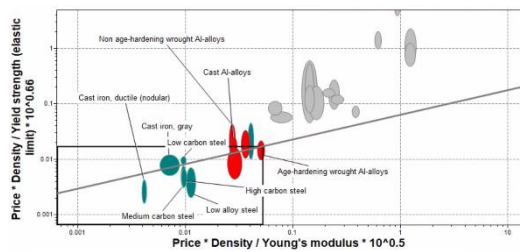


Figure 6: Cost Stiffness-Strength Constraints

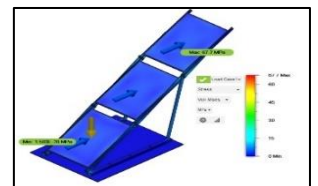


Figure 7: FEA Stress Analysis

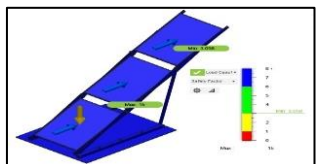


Figure 8: FEA Safety Factor Analysis

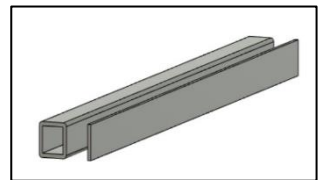


Figure 9: Geometry Iteration

4.3 Joints and Fixings

Multi-Purpose Sleeve Bearings, secured by retaining rings, were used to link all the bars in the scissor lift. Sleeve bearings allow for low-friction motion keeping maintenance to a minimum (requirement 22). They also help to reduce wear, and provide damping, which reduces vibrations and noise (requirement 12). Furthermore, MPS Bearings can withstand high axial-radial loads which is important for situations with high-winds (requirement 6). They were installed using an interference fit, preventing jamming or binding. For this application, the appropriate interference range is 0.025mm-0.076mm. A shaft basis of p6/H7 and a hole basis of H7/p6 was used. For a bearing with a nominal bore diameter of 20mm, the tolerance range is 20.0220mm-20.0350mm. From the McMaster-Carr catalogue on Fusion, bearing model 7811K224 was used. Retaining rings are suitable for secure fastening at a cost-effective price. They were installed using pliers, which widen them to allow for fitting around the sleeve bearings, and then compress them for a secure fit. From the McMaster-Carr catalogue, retaining rings with model 91032A107 were used.

5.0 Damper Selection

Dampers are a useful component used in lifting mechanisms to absorb impact forces and control their velocity by dissipating the kinetic energy of moving parts. In a vehicular lifting mechanism, external impact forces frequently occur which can potentially damage the product and be a safety hazard. Shock loads and collision forces can generate instantaneous, high impact forces which can leave significant damage and reduce the lifespan of the product. Owing to requirements 14, 20 and 23, dampers are an important device to have in our design. Below is a comparison between a linear compression damper and a rotational damper.

5.1 Linear Compression Damper

A linear damper would fit between the base joint and the bars which join the sides of the solar panels using connecting rods. According to the damper catalogue ASRaymond [7], the specific application requires a cylinder length of 300mm. Shortlisting the applicable dampers based on this, the catalogue provides the following options:

Table 6: Linear Damper Options

Product	Stroke (mm)	Base Cylinder Length (BL) (mm)	Damping Coefficient (40LBS-F / 180N Applied Load) (in/sec)	Thread (T)
DA-400V-CJ	101.600	275.08	0.4	M6 x 1.0
DA-400V-CD	101.600	275.08	0.6	M6 x 1.0
DA-400V-CE	101.600	275.08	0.8	M6 x 1.0
DA-400V-CF	101.600	275.08	1.0	M6 x 1.0
DA-400V-CS	101.600	275.08	1.4	M6 x 1.0
DA-300A-DE	76.8	218.44	3.8	M6 x 1.0

The dampers in table 6 are all finished with Nitride and have the same thread diameter of 6mm, shown by the metric M6 x 1.0. However, the main variables here are rod diameters, stroke length and dampening rate. To provide maximum damping, the damper with a maximum value for each of these variables must be selected. According to the catalogue, the maximum rod diameter is 8.0mm, and maximum stroke length is 101.6mm which only leaves the 275.08mm cylinder length dampers. The DA-300A-DE damper has the largest dampening rate of 3.8, so this is the preferred linear damper.

5.2 Rotational Damper

The rotational damper is also considered to be fixed onto the initial countershaft in line with the motor. It does not require a connecting rod and directly contributes to handling the loading torque due to the general weight of the mechanism. It can handle rotational motion, and is also compact, satisfying requirement 2. Noise pollution is another factor which needs to be considered, according to requirement 12. Rotational dampers are quieter than linear ones as they do not have the same impact forces and can withstand very high loading torque capacities.

5.3 Final Selection

The Linear damper was selected for this application since the load torque on the motor would be very large. This would mean a large gear ratio would be expected, which would result in slow rotation and would require

either an exceptionally large or exceptionally small rotational damper to have any significant damping effect on the system acting after or before the gearbox respectively.

6.0 Mechanism Design Development

6.1 Initial Motor Analysis

To shortlist the candidate motors from the Bosch Motor catalogue [2], the only motors considered were 12VDC motors without transmission. Further shortlisting the candidates to only those allowing reversible rotations left the motors APM, NSA-I p1, NSA-I p2 and NSA-I p3. Selecting reversible motors would enable the transmission system to be simplified as a reverse transmission would not have to be designed- saving cost and weight. Modelled as an inverted pendulum with no forces except the weight of the system and a gearbox efficiency (assumed to be 0.5), Figures 10, 11, 12, 13 were produced showing each motors' time of deployment, and electrical energy used, against a range of gear ratios above their respective holding ratios. A priority was to minimize the gear ratio required, for which the NSA-I_p2 motor was ideal. It had an optimum deployment time of 8 seconds with the smallest gear ratio, due to having the highest stall torque of the candidates. A low gear ratio was essential to allow higher efficiency, save space, costs, and weight. Although the other motors were similar for time optimum gear ratios, the true efficiencies of the other motors would likely be lower as higher gear ratios cause more significant losses. NSA-I_p2 and NSA-I_p3 moved on to the next stage for further analysis. Additional reasons that favoured the NSA-I motors were the presence of a hall sensor for use in automation, and an operation mode of S3. Operation mode S3(Intermittent periodic duty) was preferable to operation types S1/S2 available on the APM motor as S3 does not require the motor to reach ambient temperature before operating, unlike S2, which allows the user to quickly retract and redeploy the system if desired. Moreover, S3 minimises heat and allows smaller sized motors which adds to savings in cost and mass. S1 is continuous duty which does not fit the system [2].

6.2 Final Motor Analysis and Damping Coefficient Selection

For further analysis, the deployment and retraction of the system were modelled with winds of 25km/h acting against the deployment and with retraction. These were modelled with the gear ratios that achieved the shortest time of deployment in the previous analysis. The gear ratio for the NSA-I p2 was 1900 and for NSA-I p3 was 2700.

Motor	Electrical Energy for Deployment (J)	Mechanical Output (J)	Efficiency %
NSA-I_p2	1706	264	15.5
NSA-I_p3	1630	265	16.3

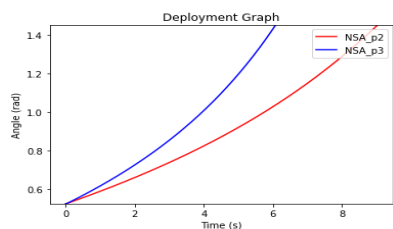


Figure 14: Angle vs Time Deployment

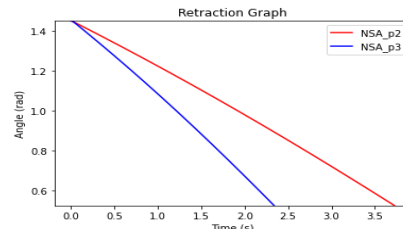


Figure 15: Angle vs Time Retraction

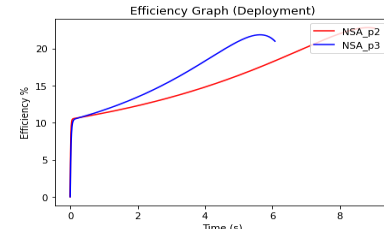


Figure 16: Efficiency vs Time Deployment

Although the motor NSA_p3 appeared to be more efficient throughout the deployment, the energy used by the two systems as shown in Table 7 was almost identical, making the NSA-I p2 motor the better choice as it requires a lower gear ratio.

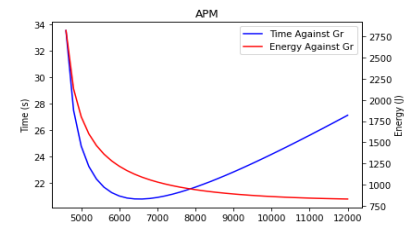


Figure 10: APM Energy and Time vs GR

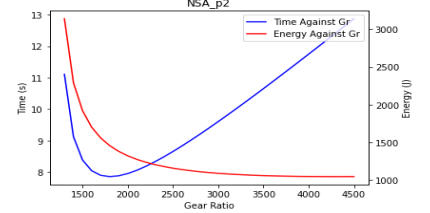


Figure 11: NSA_p2 Energy and Time vs GR

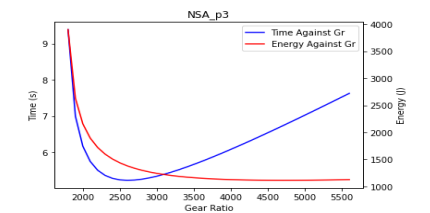


Figure 12: NSA_p3 Energy and Time vs GR

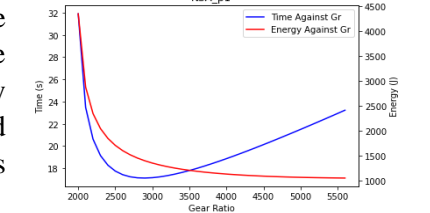


Figure 13: NSA_p1 Energy and Time vs GR

Additionally, both had deployment times within requirement 11, however the NSA-I_p2 had a slower retraction time which allowed for a lower maximum speed of the system. This would be necessary as further analysis of the system damping would find that use of typical systems of damping would hardly affect this system. Thus, the NSA-I_p2 was finally selected.

After the motor had been selected, damping coefficient selection was required. As per section 5.0, a linear damper was selected. Rotational dampers were not considered as the high gear ratio would have required a very high damping coefficient, requiring a very large and expensive rotational damper. Alternatively, the damper could have been amplified by the gearbox to achieve the desired gear ratio, however the damping coefficient required for this would have had to be too small, and would not only have been costly, but difficult to source and maintain. Two dual direction linear dampers were tested in parallel via the inverted pendulum model in the technical analysis report, each connecting a base bar to a support bar. This doubled the total damping coefficient. The candidate dampers were of the model DA-300A-CE and had total damping coefficient of 54000 Ns/m. As shown by the figures 17, 18, 19 and 20, the influence of the dampers on the system was more noticeable whilst deploying than retracting. However, the system was already at safe speeds and the payoff of having a damper was illogical as it would increase cost of manufacture, maintenance, weight, volume, and complexity. One of the main reasons that a damper was not needed was the high gear ratio. Whilst retracting, the motor would spin past the no load speed under the weight of the system and start producing resistive torque. The motor itself acted as a rotational damper. This phenomenon can be seen to begin in the retraction graphs in figures 18, 20 at the no load speed, which when calculated with the gear ratio, is approximately 0.2 rad/s and can be seen on the graph as the point where there is an immediate change in gradient.

7.0 Gearbox Design

7.1 Gear Type and Module

The gear stages included a combination of spur and worm gears. The rationale behind the decision to choose spur gears stemmed from its design simplicity. Spur gears are very cheap and easy to manufacture maintain, (requirements 20 and 22). Due to minimal sliding action between teeth, spur gears are very efficient high power transmission devices, typically ranging from 94-98% efficient. However, they are limited in their velocity ratios [9]. On the other hand, worm gears are capable of high reduction ratios (20:1 to 300:1) in a very compact space. Worm/wheels have heavy-loading applications with very quiet operation (requirement 12). A downside is that they are not very efficient with values of 40-50% due to high friction. Using both gears within the gearbox would balance the limitations and achieve the required velocity ratio in the given space.

The velocity ratio needed to be achieved was 1800-2000 as shown in the technical report. Thus, an appropriate module number for the gears had to be selected. A higher module leads to larger diameter gears which can bear more load. Additionally, the modules must be the same for meshing gears [11]. In the gearbox, the motor end where the gear stages begin has the lowest torque, whilst the loading end connected to the bars needs the highest torque. To remain compact, gears of low modules were used in the motor end which were gradually increased along the gear train, since there were gradually lower pinion speeds and higher torques. To find the modules, the maximum power values and the angular velocity of the pinions were calculated below:

$$P = - \left(\frac{T_{stall}}{\omega_{no\ load}} \right) \omega^2 + T_{stall} \omega \quad (5)$$

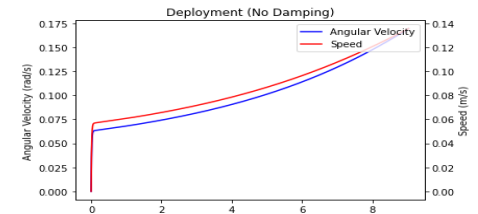


Figure 17: ω and Speed vs Time (Deployment)

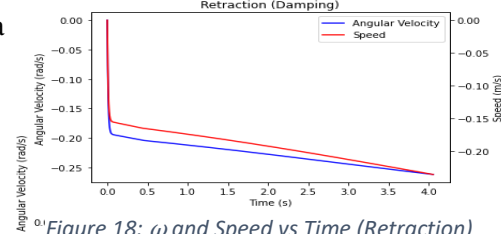


Figure 18: ω and Speed vs Time (Retraction)

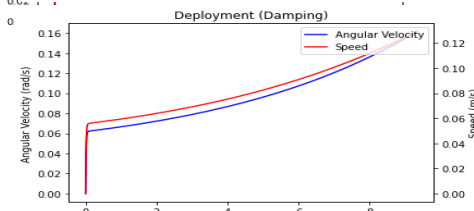


Figure 19: ω and Speed vs Time (Deployment)

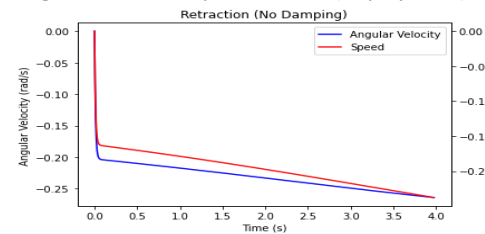


Figure 20: ω and Speed vs Time (Retraction)

Table 8: GR vs Max. Power

Gear Ratio	1800	1900	2000
Max. Power (W)	33.21	33.42	33.75

Where P is the power output, T_{stall} is the stall torque, $\omega_{no\ load}$ is no load speed, and ω is the angular velocity. Once the angular velocity was found, a gear module selection chart was used which corresponded power and pinion speed to modules. For each stage, different P, ω values and a module range of 0.5-2.5 was found.

7.2 Gear Stage Analysis

A 5-stage gear train was used to implement the velocity ratio in the most compact way, keeping low mass and cost priorities. The spur gear ratio used was 2.4-4:1 whilst the worm ratio was 25:1. The chronology of the train was 4:1 (spur), 2.4:1 (spur), 4:1 (spur), 2:1 (spur), 25:1 (worm). Any larger ratios, and the gears would not satisfy the gearbox dimensions. Consequently, the multi-stage system generated more friction which reduced the total efficiency. A trade-off was done between the conflicting variables to justify this train.

Taking into consideration the different modules used in different stages, the total number of teeth in the 5-stage configuration was 490, including pinions with maximum diameter of 120mm. If a single-stage system teeth number is to be approximated with this, the gear diameter which would not fit the gearbox dimensions. The selected gears had different bore diameters which called for varying layshafts bore diameters. The diameters ranged from 4mm-15mm. However, a limitation of this gear setup was that when the gears meshed, the same section of the gears intersected, causing concentrated wear. To solve this problem, tooth hunting was used. The improved gear ratios were found to be 25:1 (worm), 65:16, 58:25, 65:16, 53:26 which amounts to a total ratio of 1951.27 which was within the range. Additionally, the number of starts in the worm was chosen as 2. The high start value corresponded to an increase in efficiency due to increased contact area. Using the equations 6 and 7, it was found that increasing the number of individual worms increases the efficiency:

$$\eta = \left(\frac{\tan \varphi}{\tan(\theta + \varphi)} \right) \times 100 \quad [6]$$

$$\theta = \tan^{-1} f \quad [7]$$

Where η is the worm and wheel efficiency, f is the coefficient of friction and φ is the lead angle.

7.3 Gear Features, Manufacturer and Calculations

The Kohara Gear Industry (KHK) [5] was chosen as the main gear supplier due to their production of spurs and worms/wheels. Additionally, HPC gears were used as an alternative manufacturer to provide the exact cost of the gears used. This provided an estimate for the bill of materials. As for the material used in the gears, SUS303 Steel, S45C Steel, FC200 Grey Cast Iron were used. Steel is extremely abundant and has a high strength-weight ratio. Cast Iron is very cost-efficient and wear resistant. Finally, a bespoke flange was made with a hexagonal bore hole and four hexagonal head screws. The flange was screwed into the hind bar and connected to the hexagonal output shaft of the gearbox.

Table 8: Gearbox Stage Calculations

Gear Stage	1	2	3	4	5	Gear Stage	1	2	3	4	5	Gear Stage	1	2	3	4	5
VR	4	2.4	4	2	25	$\eta / \%$	96	97	96	98	61	Wheel Speed/RPM	401	167	42	21	0.84
Combined VR	4	9.6	38.4	76.8	1920	Combined $\eta / \%$	96	93	89	88	53	Pinion Speed/RPM	1604	401	167	42	21
Wheel Teeth	120	120	60	30	50	Pin. Teeth/Worm Starts	30	50	15	15	2	Wheel Torque/Nm	1.66	4.0	16	32	800
Wh. PCD/mm	60	120	120	75	101	Pin. PCD/mm	15	50	30	37.5	31	Pinion Torque/Nm	0.415	1.66	4.0	16	32
Wh. Bore Diameter/mm	10	12	15	15	15							Wh. Torque After Losses/Nm	1.6	3.7	14	28	426
Pinion Bore Diameter/mm	5	10	12	15	14							Pin. Torque After Losses/Nm	0.415	1.6	3.7	14	28

8.0 Bill of Materials

Table 9: Bill of Materials Table

Part Name	Part No.	Source	Quantity/No.	Cost per unit/(£)	Total Cost/(£)
Solar Panel	STP045BP	SolarTechnology	3	530	1590
Base Plate (Bespoke)	Bespoke	Manufactured	1	12.39	12.39
Panel Support Bar	Low Alloy Steel 4140	Metal Supermarkets	6	2.07	12.42
Deploying Bar	Low Alloy Steel 4140	Metal Supermarkets	2	2.42	4.84
Mounting Bar	Low Alloy Steel 4140	Metal Supermarkets	2	23.57	47.14
Scissor Member Bar	Low Alloy Steel 4140	Metal Supermarkets	4	2.08	8.32
Scissor Half Member Bar	Low Alloy Steel 4140	Metal Supermarkets	2	1.18	2.36
Sleeve Bearing	7811K224	McMaster-Car	18	8.40	151.2
Flat Head Screw	92010A546	McMaster-Car	12	0.76	9.12
Hex Head Screw	90854A324	McMaster-Car	6	5.87	35.22
Oval Head Screw	90258A214	McMaster-Car	3	0.088	0.264
Retaining Ring	91032A107	McMaster-Car	25	0.40	10
Flange (Bespoke)	Bespoke	Manufactured	1	34.15	34.15
Steel Spur Gear, Bore 5mm	SUSF0.5-30	KHK	1	16.54	16.54
Steel Spur Gear, Bore 10mm	SUSF0.5-120	KHK	1	15.26	15.26
Steel Spur Gear, Mod = 1	SUS1-50	KHK	1	14.74	14.74
Steel Spur Gear, Bore 12mm	SUS1-120	KHK	1	17.48	17.48
S45C Spur, Mod =2	SS2-15	KHK	1	20.29	20.29
S45C Spur, Bore 15mm	SS2-60	KHK	1	26.37	26.37
S45C Spur, Mod=2.5	SS2.5-15	KHK	1	31.83	31.83
S45C Spur, Pitch 75mm	SS2.5-30	KHK	1	35.61	35.61
Worm Wheel	CG2-R2J15	KHK	1	38.28	38.28
Worm Shaft	SW2-R2J14	KHK	1	19.37	19.37
Total					2153.20

9.0 Final Design Evaluation

Table 11 outlines the Project Solution Specification which includes major design requirements that the project met in the end as given in the PDS. Initially, the conceptualization and design stage consisted of Lego-building, CAD-sketching, and Python modelling. Many designs were tried and tested using the mentioned tools, which finally resulted in the selection of four viable designs to analyse which adhered to the given assumptions and brief. The selected concept had to establish a detailed mechanism design, so an in-depth material selection and FEA analysis was carried out to choose viable materials and beam geometry, satisfying the PDS priorities. However, many assumptions were made throughout the modelling process, which would require rigorous experimentation and real-life prototyping. The report largely focused on structural feasibility versus functional. Moreover, due to stringent requirements analogue electronic systems not be integrated into the system which would enhance the overall performance. Also, for the motor/gear selection, improving the selection process by considering more combinations might have yielded a better design. Overall, although the design had flaws it did cover important specifications and thus was a good proof-of-concept.

Table 107: PSS (Project Solution Specification) Table

PDS Requirement	PDS Target	Result	PDS Requirement	PDS Target	Result
1,2,3	1567x1108mm, 90% surface area, deployed height 1600mm, undeployed 1000mm	1400x1100mm, 100% deployed 1588mm, undeployed 950	13	300kg	240kg
4	25-40° deployed	30°	14,15,17	Obstructions	Targets met
5	12V for deployment	Target met	18,19	Sustainability	Targets met
6	120kmph winds	Target met	20	Maintenance	Target met
7	Minimum linkages, 1 12 VDC motor	Target met	21,23	Reliability	Targets met
8,9	Solar Panels detachable, compatible with standard	Target met	22	700GBP	563.2GBP
10	Automated deployment	Target met	11,16	15s, 20mph	9s, target met

References

- [1] Ansys (CES) Granta EduPack | Software for Materials Education. [online] Available at: <https://www.ansys.com/en-gb/products/materials/granta-edupack>. [Accessed 1 April 2023]
- [2] Bosch-ibusiness.com. 2022. [online] Available at: <https://www.bosch-ibusiness.com/media/images/products/dc_motors/xx_pdfs_2/pac_i-buisness_e-motors_21_22_cat_en_cd2016_82263.pdf> [Accessed 28 April 2023].
- [3] Kepler's Guide to Cascade Lifts. [online] Available at: <https://www.youtube.com/watch?v=mFs7dCj2qqE> [Accessed 3 May 2023].
- [4] Kepler's Guide to Scissor Lifts. [online] Available at: https://www.youtube.com/watch?v=ZciULF3zJvM&ab_channel=KeplerElectronics [Accessed 25 February 2023].
- [5] Kohara Gear Industry Co.,Ltd., "Involute Gear Profile," 2021. [Online]. Available: https://khkgears.net/new/gear_knowledge/gear_technical_reference/involute_gear_profile.html#:~:text=The%20condition%20for%20no%20undercutting%20in%20a%20standard,strength%20and%20contact%20ratio%20pose%20any%20ill%20effect.. [Accessed 29 April 2023].
- [6] Mitsubishi L200." [online] *Mitsubishi Motors UK*, <https://mitsubishi-motors.co.uk/cars/l200/>. [Accessed 15 February 2023]
- [7] Raymond, A., 2022. Dampers: SPD n-Struts® - Motion & Speed Control Dampers | Associated Spring Raymond. [online] Assocspring.co.uk. Available at: <<https://www.assocspring.co.uk/dampers.html>> [Accessed 15 April 2023].
- [8] Snider, C., 2023. Engineering Practice Summative Project 2023.
- [9] Spur Gears - A Complete Guide. [online] Available at: <https://uk.rs-online.com/web/content/discovery/ideas-and-advice/spur-gears-guide>. [Accessed 1 May 2023]
- [10] The Automobile Stakeholders you need to know. [online] Available at: <https://www.linkedin.com/pulse/automobile-stakeholders-you-need-know-iyamu-mohammed/>. [Accessed 23 February 2023]
- [11] The Module of a Gear. (n.d.). Available at: [https://fab.cba.mit.edu/classes/863.09/people/cranor/How_to_Make_\(Almost\)_Anything/David_Cranor/Entries/2009/10/12](https://fab.cba.mit.edu/classes/863.09/people/cranor/How_to_Make_(Almost)_Anything/David_Cranor/Entries/2009/10/12) [Accessed 1 May 2023]
- [12] What different kinds of convertible roof exist? [online] Available at: <https://www.carkeys.co.uk/guides/what-different-kinds-of-convertible-roof-exist> [Accessed 3 March 2023].



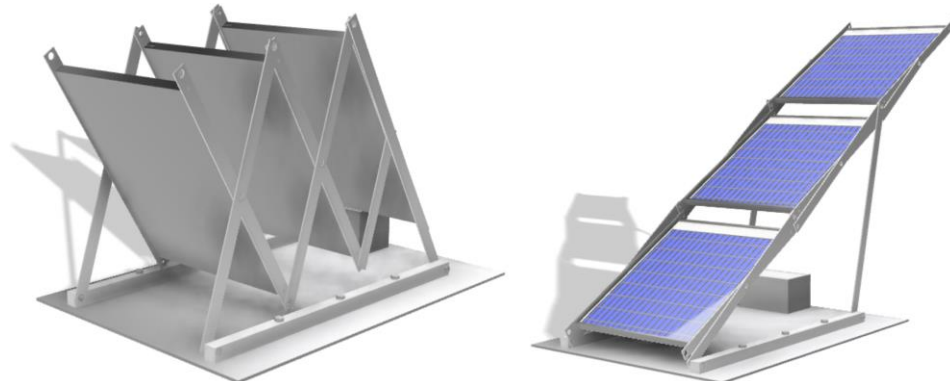
University of
BRISTOL

Mitsubishi L200 Solar Panel Deployment Platform Manufacturing Portfolio

Abdullah Monnoo (ul21823), Ibrahim Arekat (wq21745), Kabeer Dayal (pb21912), Ein Lertnawapan (fm21936)

Group 7

Report Date: 04/05/2023



1.0 Manufacturing Considerations

1.1 Workpiece Selection

The chosen bespoke component was a baseplate that acted as a platform for the deployment mechanism. This component securely fastened the scissor lift mechanism to the floor of the truck storage space. Choosing a manufacturing method involved considering the workpiece material, overall cost (requirement 22), precision, design complexity (requirement 7) and production speed. Based on the material selection process in the design portfolio, Low Alloy Steel was chosen to be used for the bars. Thus, it was determined that a workpiece of the same material was suitable for the plate. To specify the dimensions of the stock material, industry-standard plates that are readily available in the market were analysed and compared to the exact base dimensions of the existing lifting mechanism. Since flat sheets have a maximum thickness of 6.35mm [1], they were not considered. The dimensions of the scissor lift mechanism at the base was 1320mm x 823mm, and thus to keep a healthy margin, the intended base plate dimensions were chosen to be 1475mm x 1100mm to allow for any fixtures and clamping, as well as gearbox placement. To reduce cost, the 2000mm x 1250mm x 10mm plate was chosen, due to being the smallest available option which accommodates the scissor lift base dimensions. The thickness of the plate was kept as 10mm as FEA analysis in the design portfolio showed a normal pressure acting down due to the mass having a magnitude of approximately 66MPa which the Low Alloy Steel plate can comfortably resist, considering its high tensile and compressive stress resistance values. Additionally, Low Alloy workpieces are available in different heat-treated conditions for added strength [2]. Ultimately, a 4140 Steel plate workpiece was chosen and sourced.

1.2 Manufacturing Method Selection

Fabrication, CNC Machining, Casting and Forging were considered as manufacturing methods to achieve the required member geometry [7].

Table 1: Manufacturing Method Comparison

Manufacturing Process	Precision	Cost	Material Options	Design Complexity	Production Speed
Fabrication	Moderately High: Accurately carries out cutting, bending, and welding	Moderate: Depends on labour, materials, and equipment	Wide: Metals, plastics, and composites	Moderately High: Can create complex structures and assemblies	Moderate: Varies based on complexity, volume, and workforce
CNC Machining	Very High: Computerized system achieving high precision and tight tolerances	Moderate: Depends on machine setup, tooling, and labour	Wide: Metals, plastics, and composites	Very High: Complex geometries and internal features can be created	High: High machine speed and low complexity of required plate
Casting	Moderate: Dependent on mould quality and materials	Moderate: Depends on machine setup, tooling, and labour	Wide: Metals, plastics, and composites	Moderate: Limited by mould design and parting lines	Low: Mould preparation, cooling time and volume
Forging	Moderate: Dependent on dies, temperature, and material	Moderate: Dependent on tooling, labour, and material cost	Moderate: Limited by forgeability	Low: Limited by dies	Low: Die preparation, heating, cooling, and volume

It is clear from the above comparison that CNC machining is the overall best manufacturing method to achieve good control over surface finish and tight interference tolerances. The tooling material used for the milling process was chosen to be High Speed Steel (HSS) [4] which is comparatively cost efficient, and more tough and wear resistant than Carbides and Ceramics. An outline of the step-by-step machining process is elaborated below [3]:

Workpiece Preparation: Workpiece was closely inspected for any deformations, irregularities, or defects, which were removed. The workpiece was squared, ensuring that it was flat and parallel. The workpiece was securely clamped to the CNC machine's worktable, so that it was properly aligned and rigidly held in place.

Toolpath Generation: CAM (Computer-Aided Manufacturing) was used on Autodesk Fusion 360 to generate the toolpaths necessary for machining the plate. HSS was selected, for its continuous rapid cutting in ferrous materials. The machining operations were also set up, including roughing, semi-finishing, and finishing passes, as well as the fillet machining. No passes were added for depth, as the workpiece had the required depth of the plate. Multiple passes were not added to reduce operation time, since CNC is cost-rated by the hour [6]. Fillet machining was done by replacing the face mill with a 5mm radius tool. The stock was flipped over, and the process is repeated. According to Fusion 360, the estimated machining time was 13 minutes and 27 seconds.

CNC Setup: The required machining and cutting tools were installed into the CNC machine. The work coordinate system was set up and tool offsets were specified to ensure avoiding misalignments. The toolpaths generated in Fusion were loaded into the CNC controller. The specified machining process was then initiated.

Workpiece Inspection: A detailed inspection of the finished plate was carried out for accuracy, dimensions, and surface finish. Then, post-processing i.e., deburring was performed using a 76mm deburring brush on both sides to rule out any imperfections. Finally, an H7 tolerance was used to drill 6 holes to fit M20 x 70mm 45-degree countersunk screws, in order to allow for attachment between the base plate and mounting bars, as shown in the assembly and bespoke component technical drawings. The holes were made using a reamer for its high-quality finish.

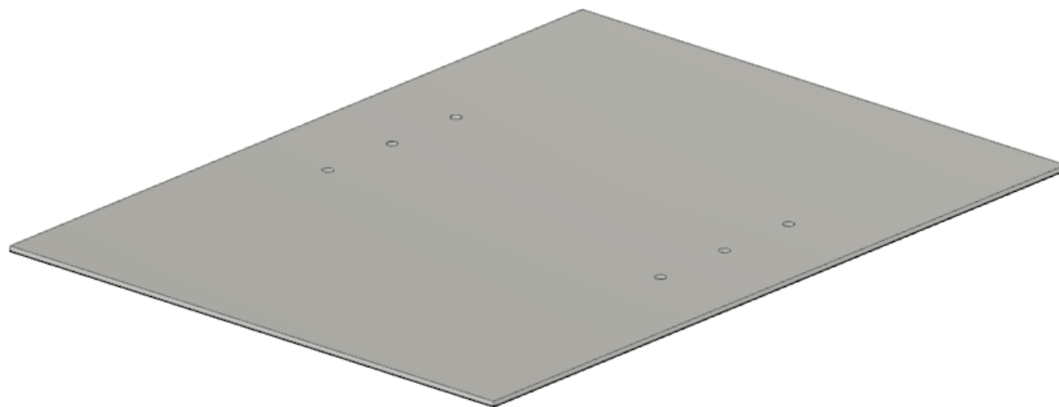


Figure 1: CAD model of low alloy steel baseplate

2.0 Manufacturing Costs

In this section of the analysis, component costs have been considered without their assembly and overhead costs. For this scenario, assembly costs can be excluded because only one bespoke component was considered here. The overhead costs were not considered because of the assumption that a different department incurred this cost. Within component cost, the stock material cost and tooling cost were considered. According to cost estimator CustomPartNet [8], several factors were considered before achieving our component cost result. Considering a run quantity in line with workpiece demand, a defect rate of 5% and a cut charge of \$1.50/part, and a selling price markup of 10% the cost per sheet came out to be \$3.30/part. Additionally, considering the 13 minutes and 27 seconds of machining time, the cost per sheet rises by \$9.70, or £7.77/part to £12.39/part. Within tooling costs, the total comes out to be £164.89 as seen in table 2 for one year of production, assuming all parts are changed once a year. This cost does not consider bulk production for output of many scissor lift mechanisms, which would decrease the cost per unit part. If all Mitsubishi L200 cars have this mechanism, and 64,391 cars were sold in 2022 [9], the tooling cost per part becomes GBP0.0026.

Table 2: Tooling Cost Table

Tool	Model No.	Cost (£)
Scotch-Brite™ Shaft Mounted Bristle Disc BB-ZS, 76 mm, P80 [5]	FN520002620	30.83
RS PRO HSS Twist Drill Bit, 28mm x 291 mm [5]	784-4800	71.40
RS PRO Plain Steel Hex Socket Cap Screw, DIN 7991, M16 x 60mm, 6 screws [5]	193-3425	48.07
4 Flute HSS Corner Rounding End Mills, 5mm fillet attachment [5]	060-280-40050	14.59

In conclusion, the overall cost for manufacturing the baseplate is ~£12.39.

References

- [1] Fractory. (2021). Sheet Metal - Materials, Standard Sizes & Forming Processes. [online] Available at: <https://fractory.com/sheet-metal/#:~:text=The%20thickness%20of%20sheet%20metal>. [Accessed 26 April 2023]
- [2] Anon, (n.d.). Heat treating low alloy PM steels | Gear Solutions Magazine Your Resource to the Gear Industry. [online] Available at: <https://gearsolutions.com/features/heat-treating-low-alloy-pm-steels/> [Accessed 4 May 2023].
- [3] get-it-made.co.uk. (n.d.). CNC Machining Guide | Get It Made. [online] Available at: <https://get-it-made.co.uk/guides/cnc-machining-guide#:~:text=The%20basic%20process%20can%20be>.
- [4] Lee, J. (2021). What Type of Steel is Best for Your CNC Machined Part? [online] Gensun Precision Machining. Available at: <https://www.china-machining.com/blog/cnc-machining-steel/>. [Accessed 25 April 2023]
- [5] My.rs-online.com. 2022. | RS Components. [online] Available at: <<https://my.rs-online.com/web/c/engineering-materials-industrial-hardware/anti-vibration-levelling-components/rotary-dampers/>> [Accessed 1 May 2023].
- [6] Parallel Precision. (n.d.). How Much Does CNC Machining Cost? [online] Available at: https://www.parallelprecision.co.uk/blog/how_much_does_cnc_machining_cost [Accessed 2 May 2023]
- [7] Form, D.R. (n.d.). Metal Forming Processes: Techniques, Industries, & Use Cases. [online] blog.dahlstromrollform.com. Available at: <https://blog.dahlstromrollform.com/metal-forming-processes-guide>. [Accessed 19 April 2023]
- [8] Machining Cost Estimator. [online] Available at: <https://www.custompartnet.com/estimate/machining/>.
- [9] BROGAN, G.-M. (n.d.). VFACTS: 2022 sales top the million mark. [online] GoAuto. Available at: <https://www.goauto.com.au/news/vfacts/sales-2022/vfacts-2022-sales-top-the-million-mark/2023-01-05/90063.html>.



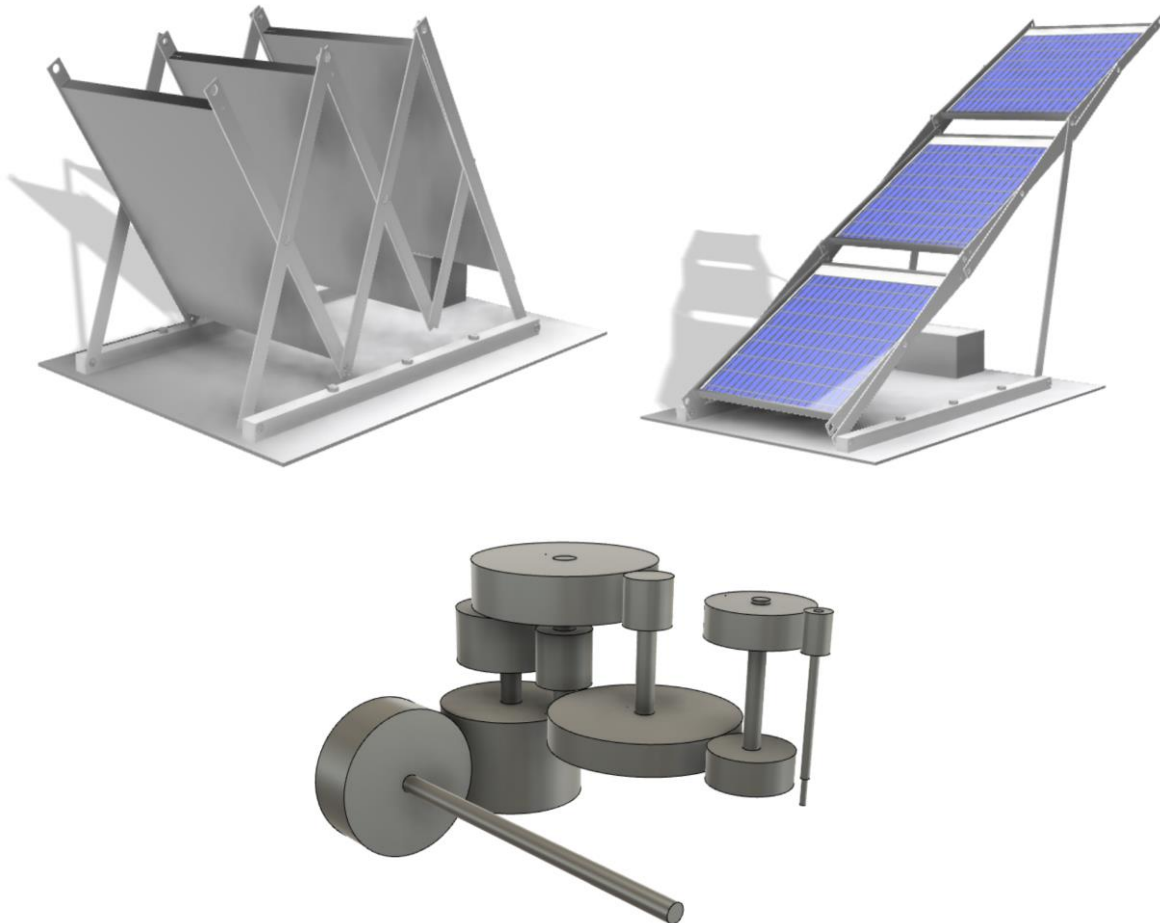
University of
BRISTOL

Mitsubishi L200 Solar Panel Deployment Platform Technical Analysis Report

Abdullah Monnoo (ul21823), Ibrahim Arekat (wq21745), Kabeer Dayal (pb21912), Ein Lertnawapan (fm21936)

Group 7

Report Date: 04/05/2023



1.0 Initial Model

An analysis of the system was based on using inverted pendulum model as shown in Figure 1. The model was based on the assumptions shown in Table 1.

Table 1: Assumptions and Effects

Assumption	Effect
MOI (Moment of Inertia) based on a point mass distance along a bar	MOI may differ based on distribution of mass relative to pivot
Friction Negligible	Since the system was slow, friction had little effect
Distance of centre of mass from pivot changes linearly with relation to angle	Relationship may not be linear
The true rotating bars were assumed to be at the same angle as the pendulum bar	This would affect the true torque required and damping.
No energy used in changing radius i.e., system force is purely rotational.	In real system, energy will be used to extend
Drag is constant when considered	The true drag would be a function of θ , and would likely increase with deployment
Coefficient of drag = 1	Coefficient is probably lesser

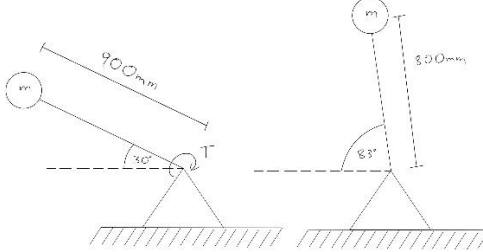


Figure 1: Inverted Pendulum Initial and Final State

First the θ_0 , θ_1 , r_0 , r_1 , were measured via the CAD model by using Fusion 360's COM function in the fully deployed and undeployed positions and measuring the distance between the main pivot and the COM. These were used to develop a linear relationship between θ and r as in Equation [1].

$$r(\theta) = \left(\frac{r_1 - r_0}{\theta_1 - \theta_0} \right) \cdot \theta + r(0) \quad [1]$$

MOI was found as that for the point mass of a pendulum in Equation [2].

$$I = m \cdot (r(\theta))^2 \quad [2]$$

These were used with the 2nd Order ODE [3].

$$\alpha = \frac{\tau(\omega) - \sum \tau_{res}}{I} \quad [3]$$

$$\tau(\omega) = \left(\tau_{stall} - \left(\frac{\tau_{stall}}{\omega_{no\ load}} \right) \cdot \omega \right) \cdot G_r \cdot \eta \quad [4]$$

$$\sum \tau_{res} = (m \cdot g \cdot \cos \theta + F_{drag} \cdot \sin \theta) \cdot r(\theta) + d_\tau(\omega, \theta) \quad [5]$$

Initially, Gearbox efficiency was assumed to be 100%, and drag force as well as the damping coefficient to be 0N. Under these assumptions, using the 4th order Runge-Kutta numerical method was used on python to solve the equation [3] while using a step size of 0.001s. Equation [6] was used to calculate power output, and Equation [7] for input.

$$P_{out} = \left(\tau \cdot \omega - \left(\frac{\tau_{stall}}{\omega_{no\ load}} \right) \cdot \omega^2 \right) \cdot \eta \quad [6]$$

$$P_{in} = V \cdot \left(\left(\tau_{stall} - \left(\frac{\tau_{stall}}{\omega_{no\ load}} \right) \cdot \omega \right) \cdot \left(\frac{\tau_{stall}}{i_{no\ load}} \right) + i_{no\ load} \right) \quad [7]$$

Integrating power with respect to time, a total efficiency was found against gear ratio. Time and efficiency were plotted against gear ratios in the figures [Figure 1](#) starting from just above the holding ratio up till 2.5x the holding ratio.

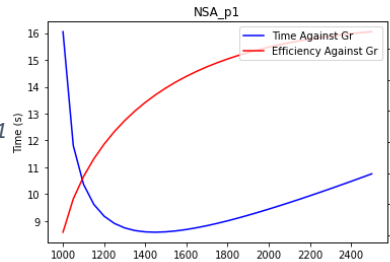


[Figure 2: NSA_p1 Time and Efficiency vs GR](#)

As shown in the figures 2,3,4 and 5, all motors achieved a similar efficiency of about 35% except for APM, achieving around 50%. NSA-I P3 had the fastest deployment time of 2.6s while NSA-I p2 followed with 4 seconds under a similar efficiency. NSA-I P1 and APM had slower deployment times and required high gear ratios so they were omitted from consideration.

From these graphs, a general idea of the required gear ratios was achieved.

2.0 Final Model and Further Analysis

After decreasing the selection of candidate motors, deeper analysis of specific gear ratios and efficiencies could be done. Since a worm gear was expected to be used to achieve these high ratios alongside spurs, gearbox efficiency (η) was assumed to be constant at 50% across all models. Final selection between the motors was achieved through simulating with aerodynamic loads and damping for deployment as well as retraction. As per requirement 6, the mechanism must be operable under winds of up to 32km/h. Aerodynamic Load at this windspeed was calculated to be 90N and modelled to act at the COM against the direction of deployment parallel to the ground. Using the ratio for the fastest deployment of each gear, the retraction of the system was modelled with the winds of 90N acting with the system on the COM point. Since it was known that the system could act against the wind load, this was modelled to ensure the system operated normally at safe speeds when wind was acting alongside it. Figures 6 and 7 show the values from the final model.

For the retraction, modified equations had to be used. For most of the deployment the motor would be above the no load speed, so the gearbox efficiency term would be multiplied with the $\sum \tau_{res}$ term rather than the motors driving torque $\tau(\omega)$.

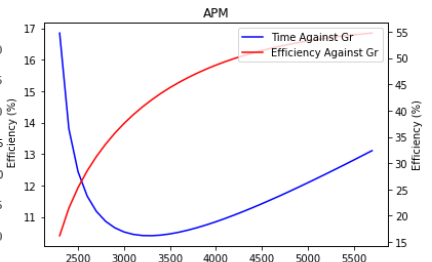


[Figure 3: APM Time and Efficiency vs GR](#)

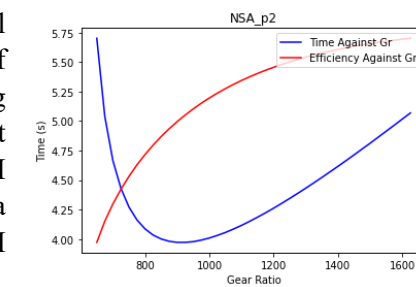


[Figure 4: NSA_p2 Time and Efficiency vs GR](#)

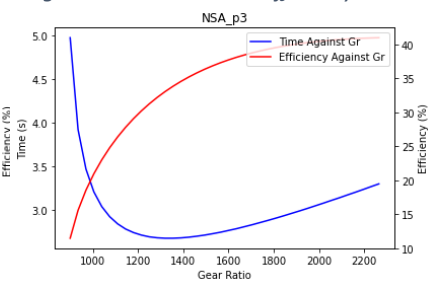


[Figure 5: NSA_p3 Time and Efficiency vs GR](#)

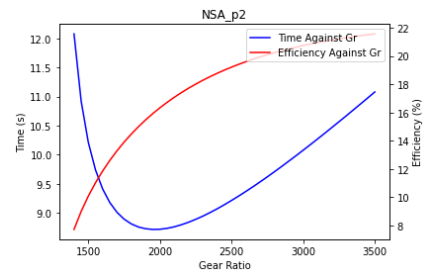


[Figure 6: NSA_p2 Time and Efficiency vs GR](#)

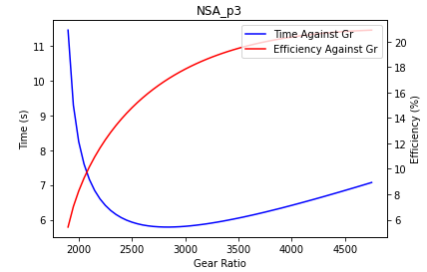


[Figure 7: NSA_p3 Time and Efficiency vs GR](#)

$$\tau(\omega) = \left(\tau_{stall} - \left(\frac{\tau_{stall}}{\omega_{no\ load}} \right) \cdot \omega \right) \cdot G_r \quad [8] \quad \sum \tau_{res} = ((m \cdot g \cdot \cos \theta + F_{drag} \cdot \sin \theta) \cdot r(\theta) + d_\tau(\omega, \theta)) \cdot \eta \quad [9]$$

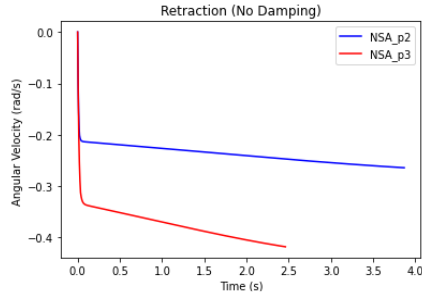


Figure 8: Angular Velocity Retraction(No Damping)

Linear Dampers were added to determine if they influenced the safety of the system in relevance to requirement 14. Figure 8 shows velocities with no damping. After manual runs of the model, a way to fix a pair of linear dampers was found which approximately achieved the maximum stroke length of the damper, thus creating the greatest effect. Thus, the linear damper was fixed to the mounting bar 0.3 (a) metres from the motor, and on the deployment bar 0.1 (b) metres from the motor. The damping coefficient d_c was set as 54000Ns/m and damping was modelled by equations [10].

$$d_\tau(\omega, \theta) = \frac{d_c \cdot a^2 \cdot b^2 \cdot \omega \cdot \sin^2 \theta}{d_{Length}(\theta)} \quad [10] \quad d_{Length}(\theta) = \sqrt{a^2 + b^2 - 2 \cdot a \cdot b \cdot \cos \theta} \quad [11]$$

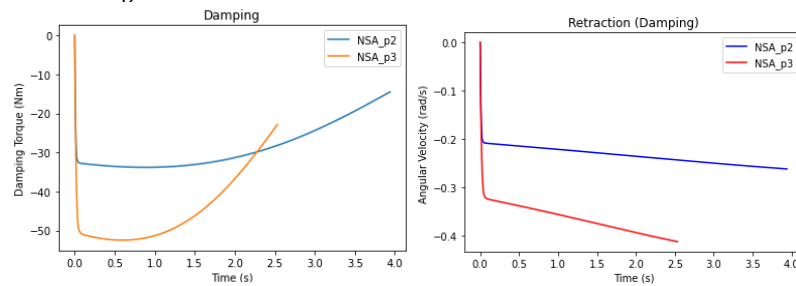


Figure 9: Damping Torque Against Time

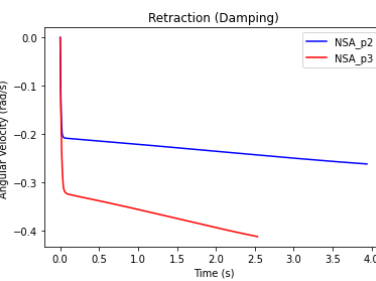


Figure 10: Angular Velocity Retraction (Damping)

As shown in figure 10, damping (figure 9) hardly had a noticeable difference except decreasing the times by approximately 0.1s. It should be noted that the motor was acting as a rotational damper, further described in the motor selection in the design report. The motor characteristic curve was then extrapolated to calculate the voltage past the no load speed via equation [12].

$$V = \frac{\omega}{\left(\frac{\tau_{stall}}{i_{no\ load}}\right)} - 2 \cdot i_{no\ load} \quad [12]$$

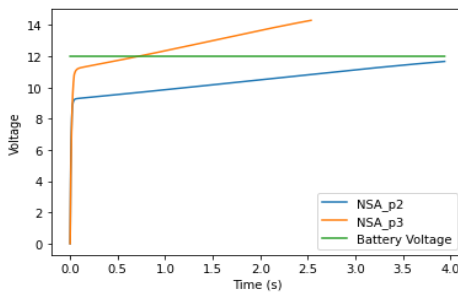
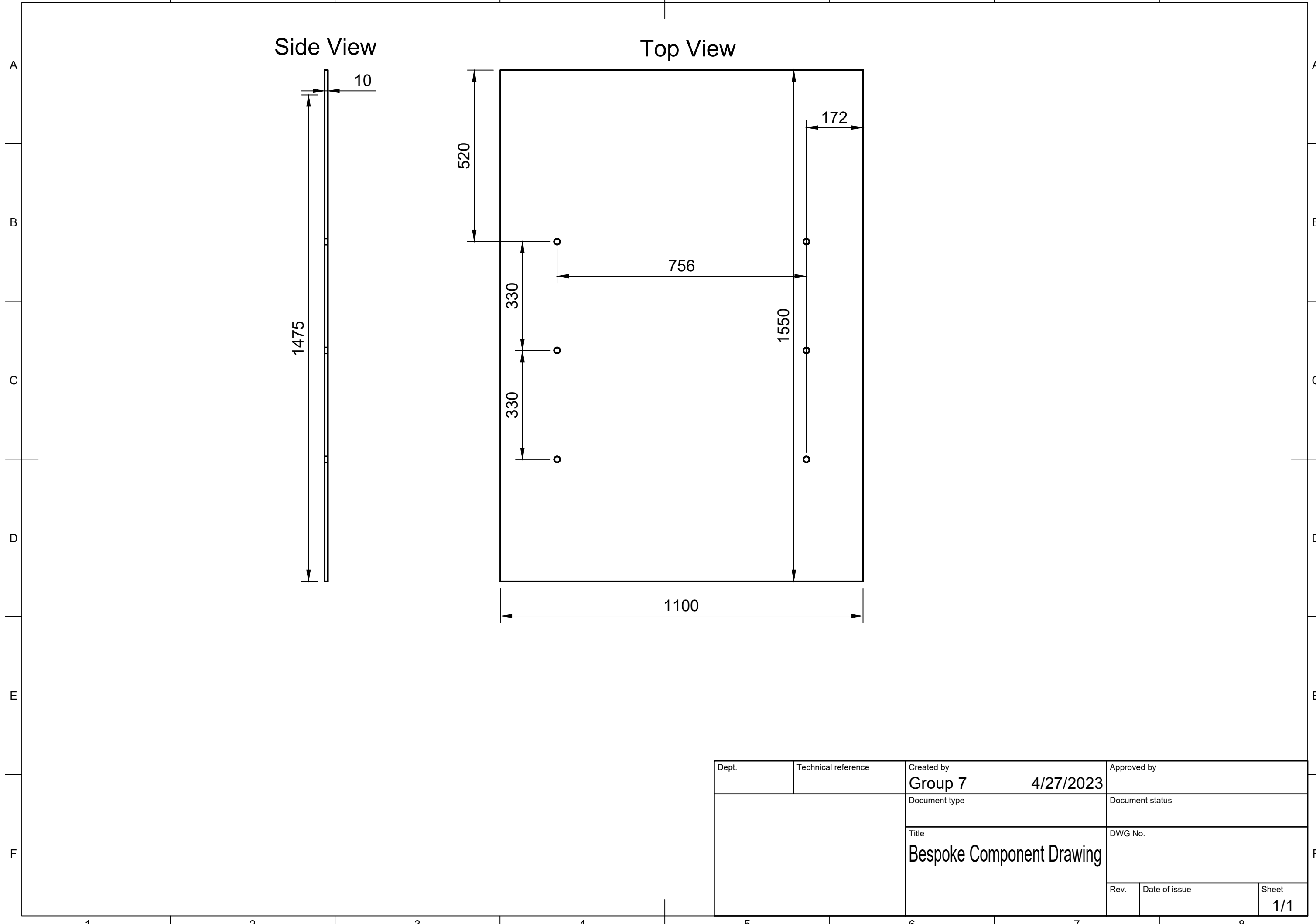


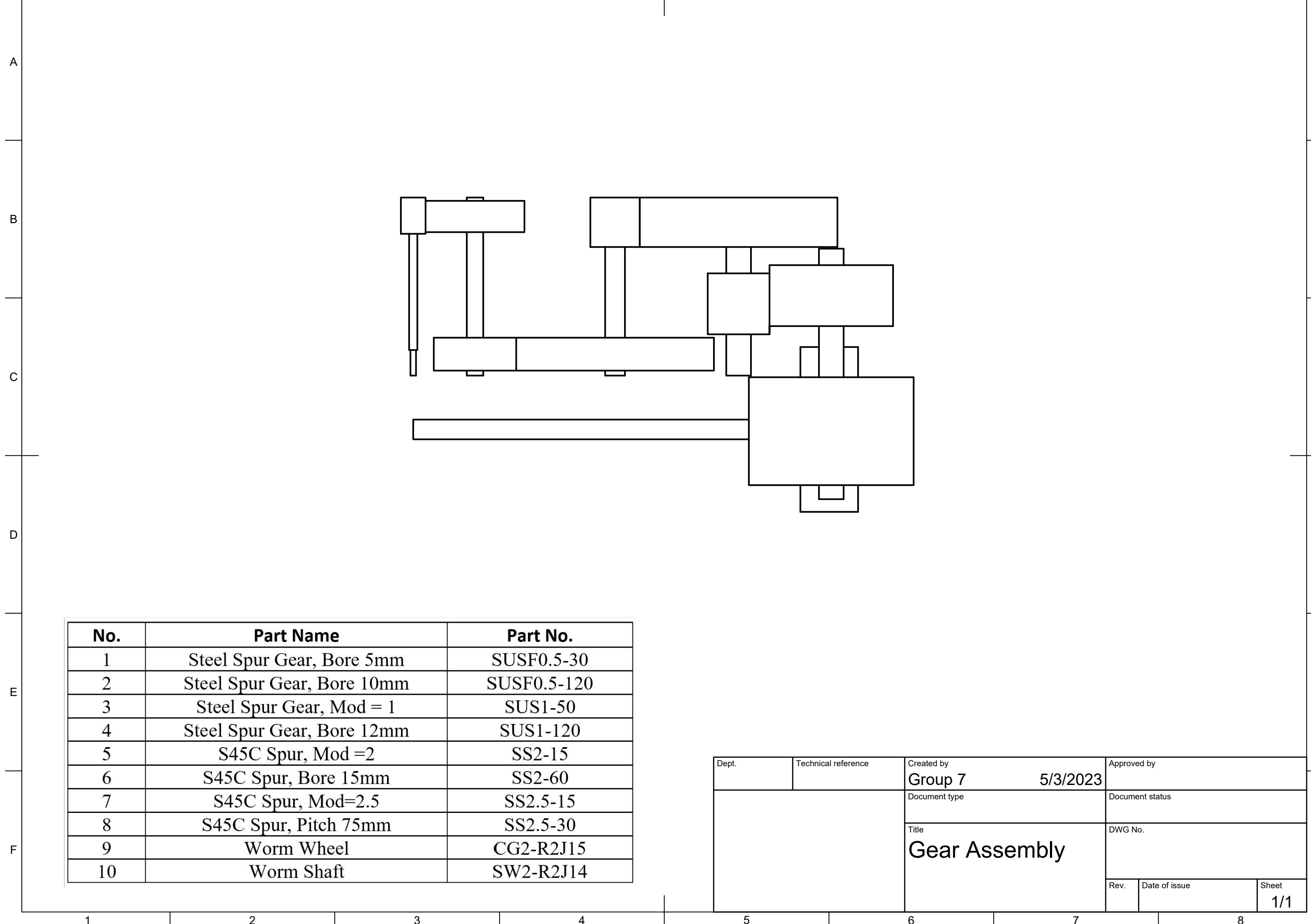
Figure 11: Voltage across motor against Time

As seen in figure 11, the NSA-I P3 would exceed the voltage supply of the battery creating a back voltage of 14V at its peak. The NSA-I P2 however would just stay below the 12V supplied by the battery. A back voltage would force countermeasures to be added against damage to the circuit. In conclusion, lower gear ratio, no back voltage and fast deployment time favoured the motor NSA-I P2.

1 2 3 4 5 6 7 8

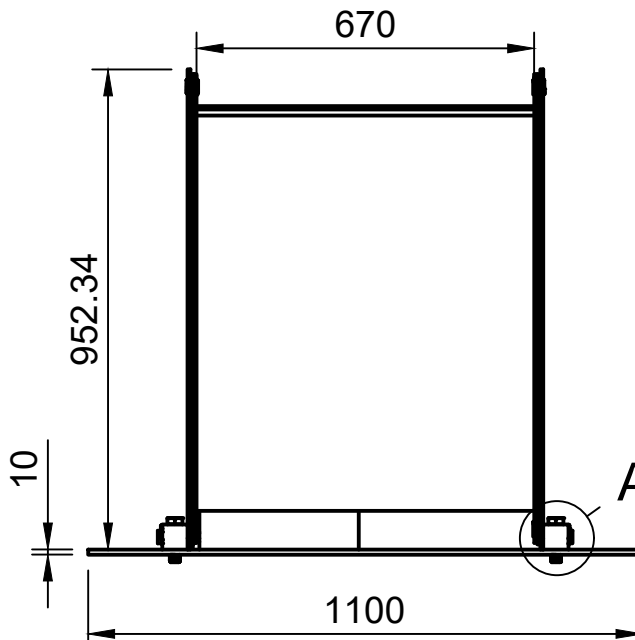


1 2 3 4 5 6 7 8

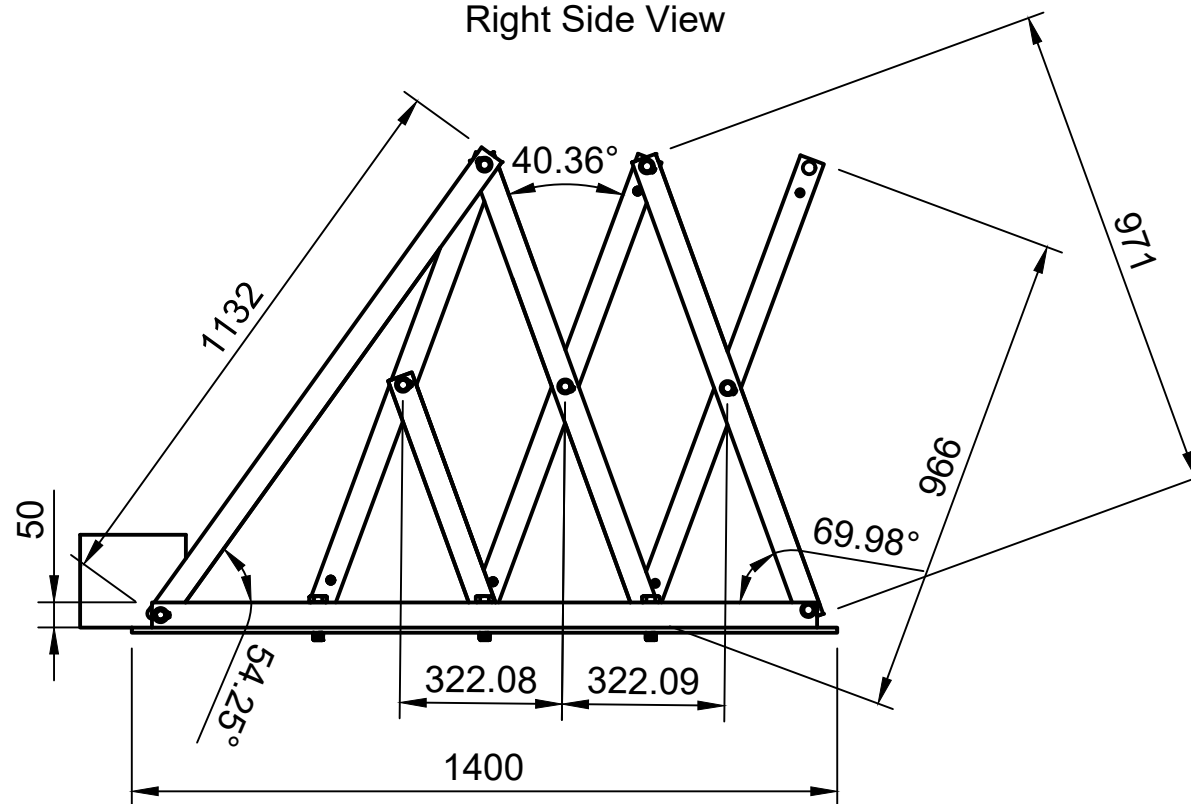


1 2 3 4 5 6 7 8

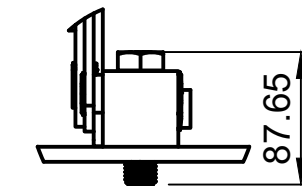
Front View



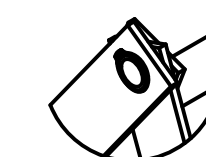
Right Side View



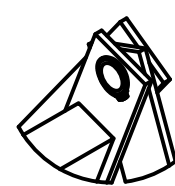
A (1:5)
M20x2.5



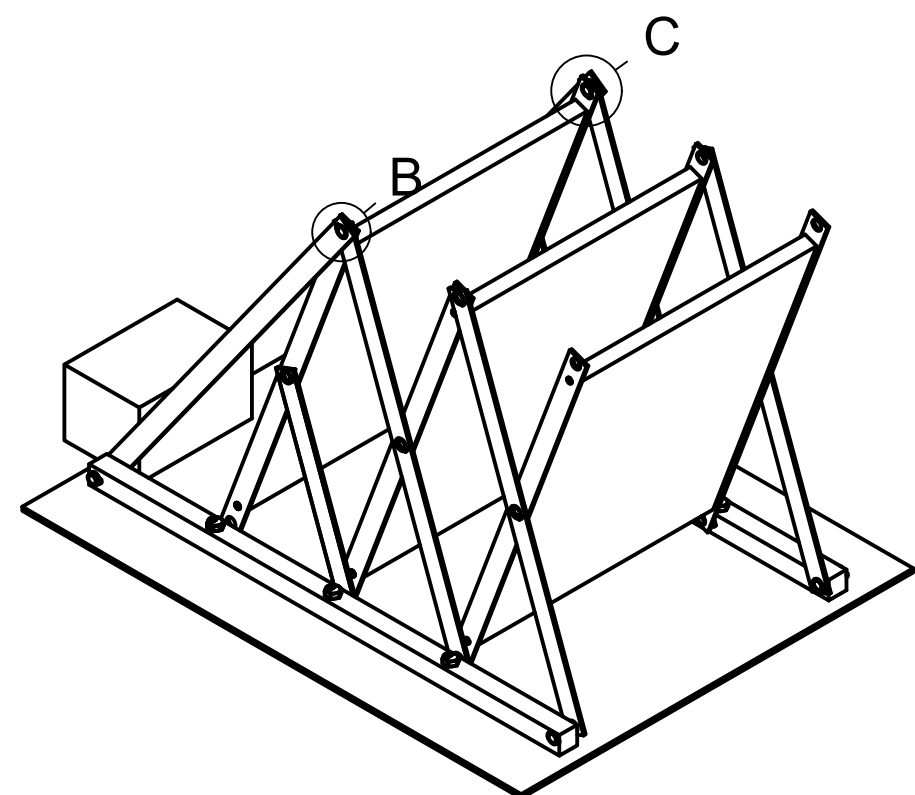
B (1:5)



C (1:5)



Isometric View



No.	Part Name (Quantity)
1	Solar Panel (3)
2	Base Plate (1)
3	Panel Support Bar (6)
4	Deploying Bar (2)
5	Mounting Bar (2)
6	Scissor Member Bar (4)
7	Scissor Half Member Bar (2)
8	Sleeve Bearing (18)
9	92010A546 Flat Head Screw (12)
10	90854A324 Hex Head Screw (6)
11	90258A214 Oval Head Screw (3)
12	91032A107 Retaining Ring (25)
13	Flange (1)
14	Gearbox (1)

Dept.	Technical reference	Created by Group 7 4/28/2023	Approved by
	Document type		Document status
	Title Solar Deployment System Assembly		DWG No.
Rev.	Date of issue		Sheet 1/1

1 2 3 4 5 6 7 8

